metals

MDPI

Article

Welding Quality Detection for Variable Groove Weldments Based on Infrared Sensor and Artificial Neural Network

Rongwei Yu [1,2,*], Yong Huang [1,2], Shubiao Qiu [1,2], Yong Peng [1,2] and Kehong Wang [1,2,*]

[1] School of Materials Science and Engineering, Nanjing University of Science and Technology, Nanjing 210094, China
[2] Key Laboratory of Controlled Arc Intelligent Additive Manufacturing Technology, Nanjing University of Science and Technology, Nanjing 210094, China
* Correspondence: yurongwei@njust.edu.cn (R.Y.); wkh1602@126.com (K.W.)

Abstract: Connecting a variable groove weldment is always challenging, and it is necessary to monitor the course of the work and optimize the welding process parameters in real time to ensure the final welding forming quality. Welding penetration is an important index to appraise the welding forming quality; the visual sensing method for molten pool is the main method for detecting the weld penetration, but its detection accuracy is affected by the arc light. In this paper, a welding penetration sensing method for variable groove weldments based on the welding temperature field distribution is proposed. Firstly, a set of temperature field measurement system for a weldment is developed by means of an infrared sensor. Secondly, in the direction perpendicular to the welding direction, a linear temperature distribution feature extraction algorithm based on Gaussian fitting is studied; in the direction parallel to the welding direction, the linear temperature distribution feature extraction algorithm based on the thermal cycle parameters is studied, and the feasibility of using the extracted linear temperature distribution features to identify the weld penetration of a variable groove weldment is analyzed. Finally, taking the extracted linear temperature distribution features as input, using an artificial neural network, the prediction model for the welding penetration of a variable groove weldment is established. The experimental results showed that the weld penetration sensing method put forward in this paper can realize high-precision weld penetration sensing and has high reliability, which solves the problem that weld penetration sensing is affected by arc light to a great extent.

Keywords: variable groove; penetration sensing; infrared sensor; Gaussian fitting; thermal cycle parameters

Citation: Yu, R.; Huang, Y.; Qiu, S.; Peng, Y.; Wang, K. Welding Quality Detection for Variable Groove Weldments Based on Infrared Sensor and Artificial Neural Network. *Metals* **2022**, *12*, 2124. https://doi.org/10.3390/met12122124

Academic Editor: Alberto Campagnolo

Received: 17 November 2022
Accepted: 6 December 2022
Published: 10 December 2022

1. Introduction

Welding is a manufacturing process and the technology of joining metals by heating, high temperature or high pressure. In recent years, the online inspection of welding quality has become a research highlight in the field of welding [1–3]. Realizing the online inspection of welding quality can find welding defects in a timely manner so as to be able to quickly adjust and optimize the welding process parameters and, finally, achieve the goals of maintaining the welding quality and improving the welding processing efficiency.

In the welding process, multisource information, such as the electric signal, vision, temperature, and spectrum, can reflect the welding quality to a large extent; therefore, the welding quality can be inspected by online sensing of the multisource information. Among them, the vision sensing method is widely used in welding quality inspection. Zhang et al. [4] studied an improved fuzzy edge detection algorithm, which can extract the weld edge from a low-contrast welded joint image, providing strong support for the detection of welding defects. Deng et al. [5] studied a weld edge extraction algorithm based on beamlet transform, which can accurately extract weld edges from high noise welding images with high efficiency. Shen et al. [6] studied two weld defect detection methods based on visual sensing and subsequently combined the two methods using

information fusion to improve the reliability of weld defect detection. Khumaidi et al. [7] established a classification model for welding defects using a convolutional neural network and Gaussian kernel, with the acquired weld image as input; it could achieve the high-precision classification of four types welds: good weld, over spatter, polarity, and undercut. Haffner et al. [8] proved that a convolutional neural network is a reliable and promising evaluation method when visual sensing is used to detect welding quality. The above documents realized welding quality detection by directly imaging the weld; in order to directly avoid the impact of arc light on welding quality detection, this paper measured the temperature field distribution of the welding heat-affected zone around the molten pool region through infrared band imaging and studied the relationship between the welding temperature field and welding quality.

The weld penetration is closely related to the welding forming quality, and many scholars have carried out in-depth research on the sensing technology of weld penetration [9–11]. Sibilano et al. [12] studied a spectrum-based laser welding penetration sensing technology, and online sensing of the welding penetration was realized through the real-time measurement of the electron temperature of the plasma. Yang et al. [13] studied a penetration sensing technology for aluminum alloy welding based on the weld pool vision, and they built a penetration recognition model based on an artificial neural network. Xia et al. [14] developed a penetration evaluation model for resistance spot welding on the basis of the electrode displacement signals, and they tested its generalization ability under different welding conditions. Ren et al. [15] established a gas tungsten arc welding (GTAW) penetration classification model for aluminum alloy based on arc sound detection and deep learning; its classification accuracy was better than many typical models. Yu et al. [16] aimed at the problem that a single molten pool image does not contain enough information to predict the welding forming quality, and they studied a welding penetration sensing technology based on a sequential weld pool image and deep learning. Liu et al. [17] aimed at the problem that the instability of small holes will affect the penetration of laser welding, and they studied a pulse laser welding penetration sensing technology using vision sensing and deep learning. To sum up, a change in the welding penetration will inevitably lead to a change in the multisource information features during the welding process. When connecting a variable groove weldment, the change in the penetration will also be reflected by a change in the welding temperature field distribution features; therefore, using the temperature information in the welding process to carry out online sensing of the welding penetration is a feasible research direction.

In order to measure the temperature information during the welding process, infrared detection is a feasible means, which is an important testing method in the field of nondestructive testing [18]. Tan et al. [19] measured the welding temperature field distribution using an infrared thermometer, modified the parameters of a double elliptical distribution heat source model, and established a finite element numerical simulation model for welding temperature field. Alfaro et al. [20] studied a GTAW defect detection technology based on infrared sensing, and they explored the relevance between the change of welding temperature and forming defects. Kafieh et al. [21] processed the infrared image sequence of a welded polyethylene pipe, which showed good performance in welding defect detection. Zhu et al. [22] developed a set of infrared visual sensing systems for detecting the weld offset of swing arc narrow gap welding. Guo et al. [23] studied an ultrasonic infrared thermal imaging technology for crack defect detection of friction stir welded joints of aluminum alloy sheets. Górka et al. [24] studied a reflection temperature correction technology to reduce the uncertainty of the absolute temperature measurement using an infrared sensor, which was used to diagnose several typical welding defects, including nonpenetration and unsatisfactory weld formation size. To sum up, infrared detection has become an important means for welding process monitoring; after infrared images are collected by an infrared sensor, they are processed using image processing algorithms so as to extract the features strongly related to welding forming quality. By identifying these features, welding quality monitoring can be realized to a certain extent.

In order to accurately establish the relationship between the signal features and welding forming quality, the outstanding performance of artificial neural networks has attracted great attention by welding workers. An artificial neural network is an important branch of machine learning, and from the relevant research results in the welding field, artificial neural networks are widely extended to welding process parameter design, welding performance prediction, and welding forming quality monitoring and control [25–28]. Luo et al. [29] determined the sound signal features that were strongly related to the welding quality and established a laser welding defect identification model using an artificial neural network. Hong et al. [30] studied a prediction technology for the weld morphology of laser arc hybrid welding using an artificial neural network. Lei et al. [31] studied a prediction technology for the geometric features of a laser welding seam using multisource information fusion, with the extracted weld pool morphological features and welding process parameters as inputs, and built a weld geometry prediction model using an artificial neural network. Li et al. [32] used a passive visual sensing system to acquire weld pool images, and they developed a prediction model for GTAW penetration using a convolution neural network. Bacioiu et al. [33] studied a tungsten inert gas (TIG) weld defect detection technology by means of high dynamic range imaging, and they established a welding defect identification model based on a convolutional neural network. Hartl et al. [34] studied friction stir welding process monitoring technology, and they used various types of artificial neural networks to detect the quality of friction stir welds. To sum up, the application of artificial neural networks in the welding field has resulted in many achievements, but there is no mature algorithm for determining the parameters of a neural network at present. Improving the generalization ability of artificial neural networks is also the focus of future research.

In this paper, welding penetration sensing technology for variable groove weldments was studied, which innovatively uses the temperature field distribution of the welding heat-affected zone around the weld pool to sense the weld penetration. The temperature field distribution of the weldment was measured by means of infrared thermal imaging, the feature extraction algorithm of the temperature distribution perpendicular and parallel to the welding direction on the weldment surface was studied, the key information such as the welding thermal cycle parameters was extracted, and the feasibility of using the extracted linear temperature distribution features to identify the welding penetration of variable groove weldments was analyzed. Finally, a back propagation (BP) neural network was adopted to establish a welding penetration diagnostic model for variable groove weldments. The welding penetration sensing method proposed in this paper does not need to observe the dynamic behavior of the molten pool but only needs to detect the temperature field distribution of the welding heat-affected zone around the weld pool, and it can achieve high-precision sensing of the welding penetration for variable groove weldments.

2. Design of the Welding Penetration Sensing System for Variable Groove Weldments

A connection experiment on variable groove weldments was conducted under a gas metal arc welding (GMAW) process. The whole welding experimental platform mainly consisted of a welding system and a welding penetration sensing system for variable groove weldments, which is shown in Figure 1. The welding system included an electric welding machine, welding gun, wire feeder, control cabinet, and protective gas; the welding penetration sensing system for the variable groove weldments included an infrared sensor, signal generator (UNI-T, UTG932), and a computer. The infrared sensor was connected to the welding gun through a clamp, and its monitoring area mainly included the welding heat-affected zone around the weld pool. At the start of the welding process, the signal generator sent a square wave signal with a frequency of 50 Hz to trigger the infrared sensor to measure the temperature field distribution on the weldment surface online. Subsequently, the temperature distribution image of the weldment was input to the computer for processing, the key information such as the welding thermal cycle parameters was extracted by the designed linear temperature distribution feature extraction algorithm and then input to

the artificial neural network model, and the penetration of the variable groove weld could be sensed online. The welding wire and weldment were made of stainless steel, and the specific welding process parameters are shown in Table 1.

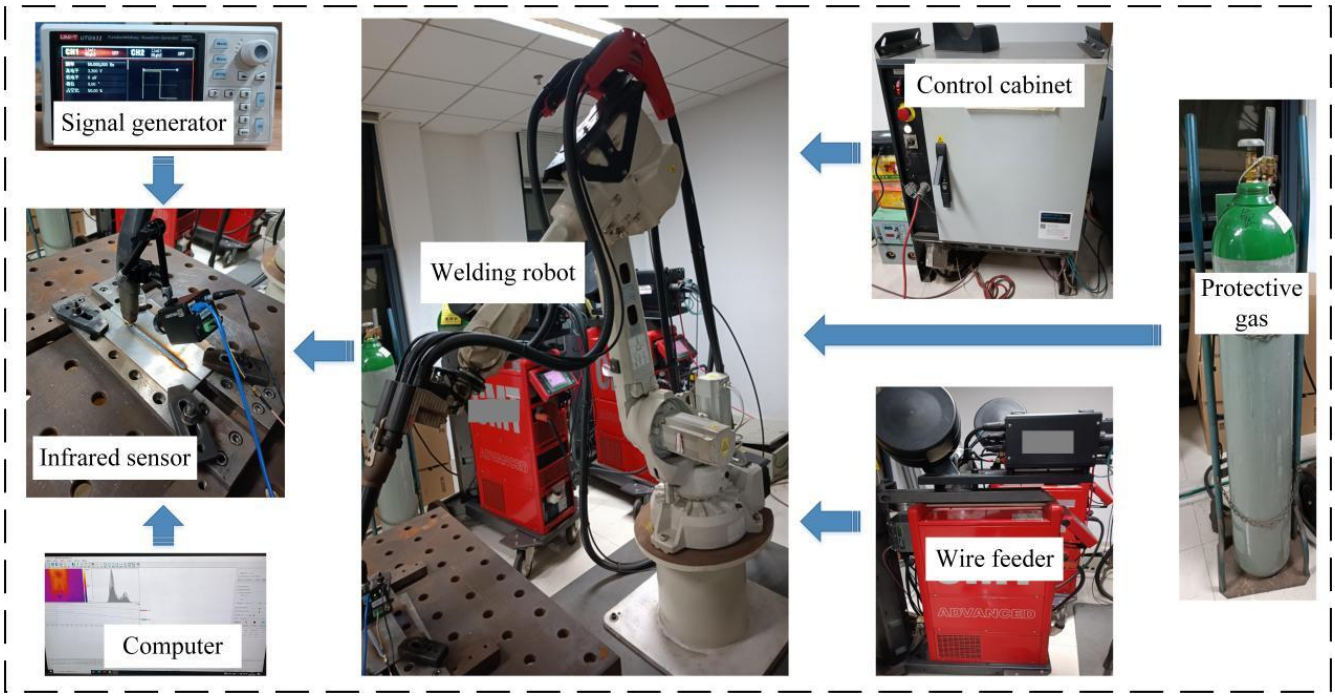

Figure 1. Welding penetration sensing system for variable groove weldments.

Table 1. Welding process parameters.

Process Parameter	Value
Welding technology	GMAW
Welding wire grade	ER316L
Welding wire diameter	1.2 mm
Weldment	304 stainless steel
Base metal size	27 cm × 6 cm × 5 mm
Base metal blunt edge	1 mm
Protective gas composition	99%Ar + 1%O_2
Protective gas flow	25 L/min
Welding current	158 A
Welding voltage	17.8 V
Welding speed	5 mm/s
Wire feeding speed	6.6 m/min

The groove angle of the weldment directly affects the welding penetration, so we processed the weldment into variable grooves along the welding direction. A structural diagram of a variable groove weldment is shown in Figure 2.

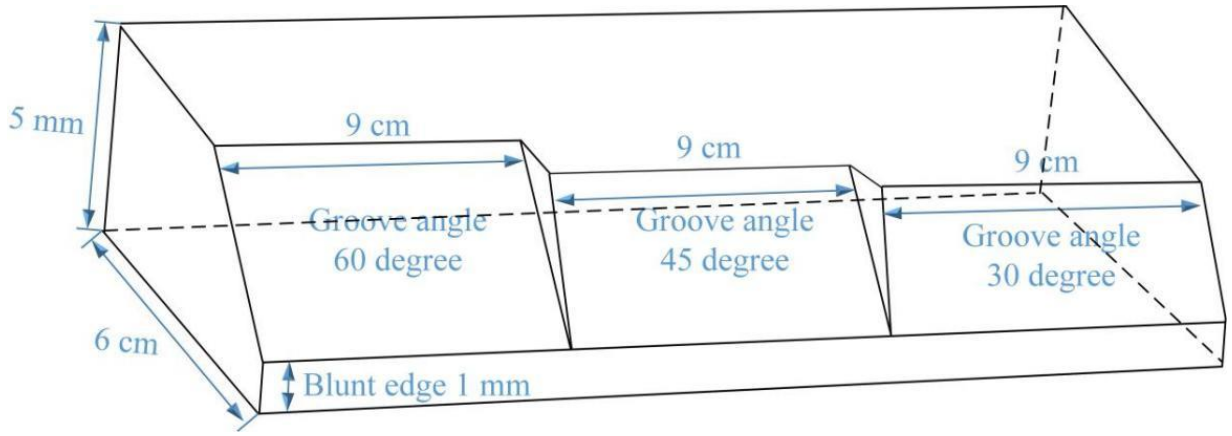

Figure 2. Structural diagram of a variable groove weldment.

The starting point of the welding was set at 4 cm from the edge of the base metal part with a groove angle of 30 degrees. In addition, the distance between the welding end point and the starting point was set at 19 cm. Setting the welding parameters in accordance with Table 1, after completion of the welding experiment, the penetration state of the variable groove weld is shown in Figure 3. It can be seen that the first 5 cm welded joint was in the mode of nonpenetration, the next 9 cm welded joint was in the mode of full penetration, and the last 1 cm welded joint was in the mode of excessive penetration. In cases where the section of the welded joint was in the mode of excessive penetration and there was a tendency of welding leakage, the welding arc was extinguished, and the welding process was stopped.

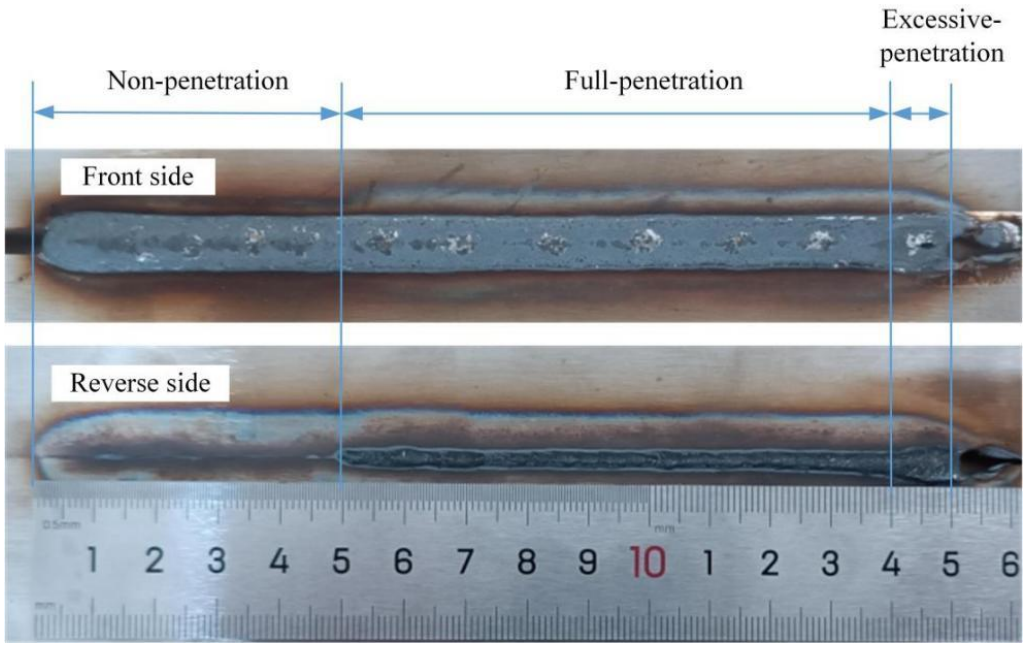

Figure 3. The penetration state of a variable groove weld.

3. Feature Extraction of the Linear Temperature Distribution on a Weldment Surface

In the welding process, the temperature field image of a weldment surface measured by an infrared sensor at different times is shown in Figure 4. When an infrared sensor is directly adopted to measure the temperature field distribution of a weldment surface, according to our previous research work [35], based on the temperature measurement principle of the infrared sensor, its temperature measurement results are related to the emissivity of the

target. The molten pool is liquid, and the welding heat-affected zone around the molten pool is solid; the emissivity of the solid and liquid is different. Furthermore, the molten pool area will be covered by arc light during the welding process; therefore, the temperature measurement results in the molten pool area are unreliable, and it is feasible to select the heat-affected zone around the weld pool area for the temperature field measurement.

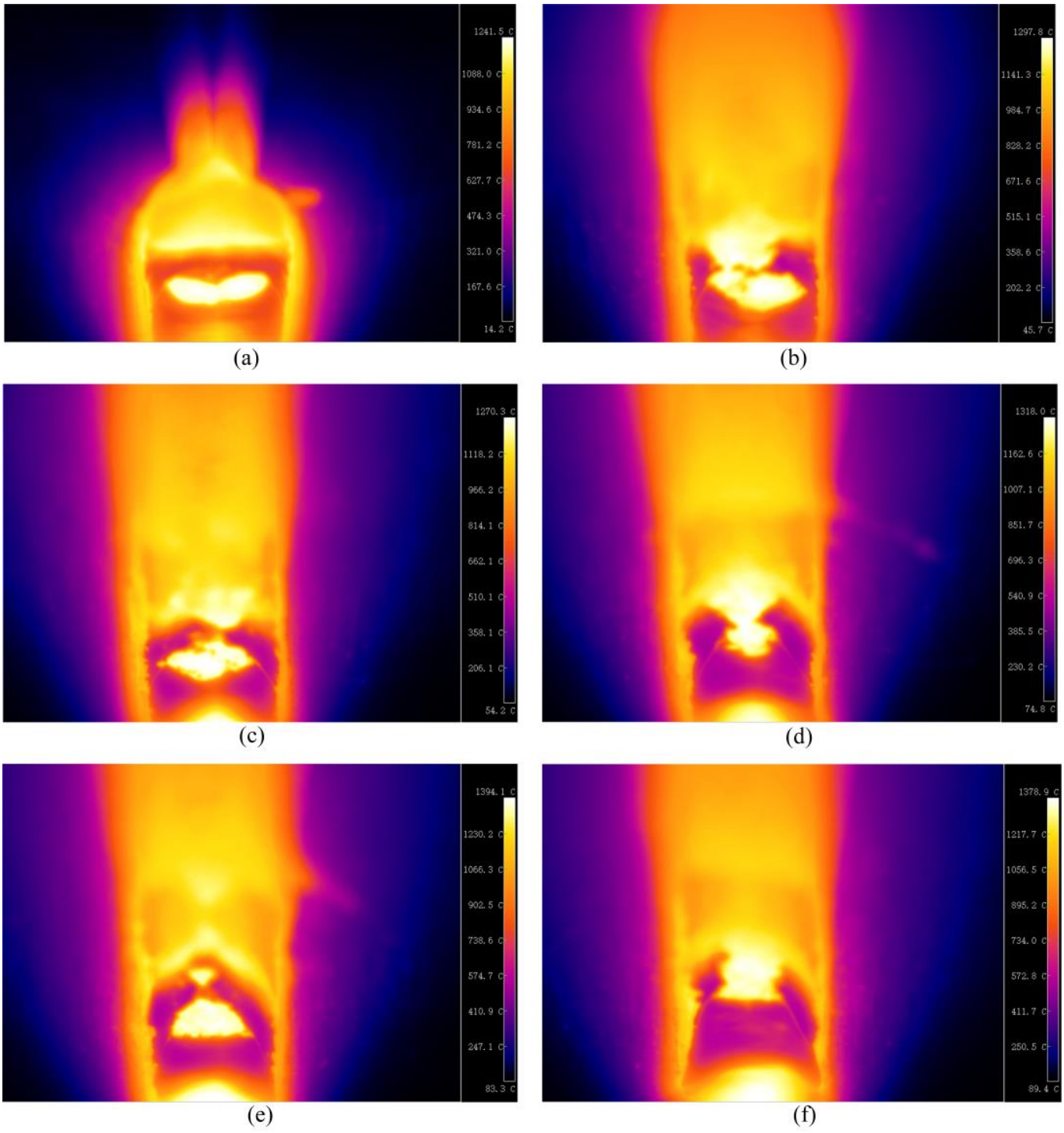

Figure 4. Temperature field images of a weldment surface measured at different times: (**a**) t = 4 s; (**b**) t = 8 s; (**c**) t = 12 s; (**d**) t = 20 s; (**e**) t = 25 s; (**f**) t = 29 s.

In order to study the distribution law of the welding temperature field under various penetration modes, taking the temperature field of the weldment surface in Figure 4 as

an example, firstly, the linear temperature distribution features of the weldment surface perpendicular to the welding direction were extracted. Figure 5 shows a schematic diagram of the selected line segments in the heat-affected zone. In this paper, a relatively fixed line segment was selected from the heat-affected zone in the measured temperature field image of the weldment surface, and the raw data on the linear temperature distribution were processed by quadratic fitting, cubic fitting, and Gaussian fitting. The function expression adopted for the Gaussian fitting was:

$$y = a \exp\left(-\left(\frac{x-b}{c}\right)^2\right) \quad (1)$$

where a, b, and c are constants; x is an independent variable; and y a dependent variable.

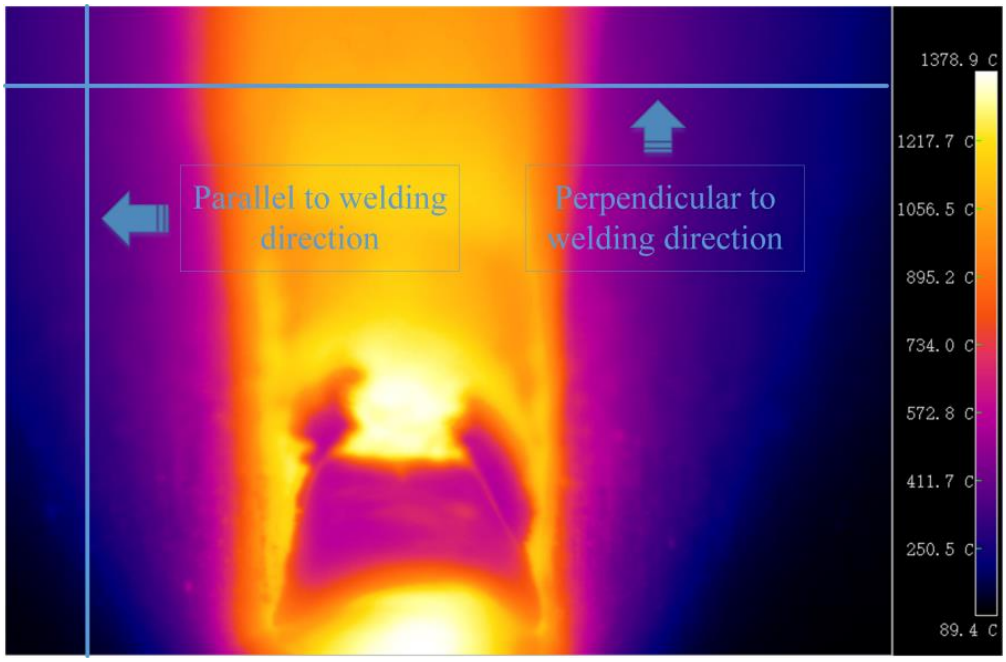

Figure 5. Schematic diagram of the selected line segment in the heat-affected zone.

Figure 6 is the Gaussian fitting result of the original temperature distribution data. The function expression after the fitting shown in Figure 6a was $y = 162.8683 \exp\left(-((x-178.4872)/122.3834)^2\right)$; the function expression after the fitting in Figure 6b was $y = 869.3238 \exp\left(-((x-174.3964)/129.1515)^2\right)$; the function expression after the fitting in Figure 6c was $y = 907.036 \exp\left(-((x-167.0896)/130.2656)^2\right)$; the function expression after the fitting in Figure 6d was $y = 950.2439 \exp\left(-((x-165.3563)/128.9623)^2\right)$; function expression after the fitting in Figure 6e was $y = 949.0039 \exp\left(-((x-167.4753)/129.8019)^2\right)$; the function expression after the fitting in Figure 6f was $y = 954.0581 \exp\left(-((x-167.5125)/132.1399)^2\right)$.

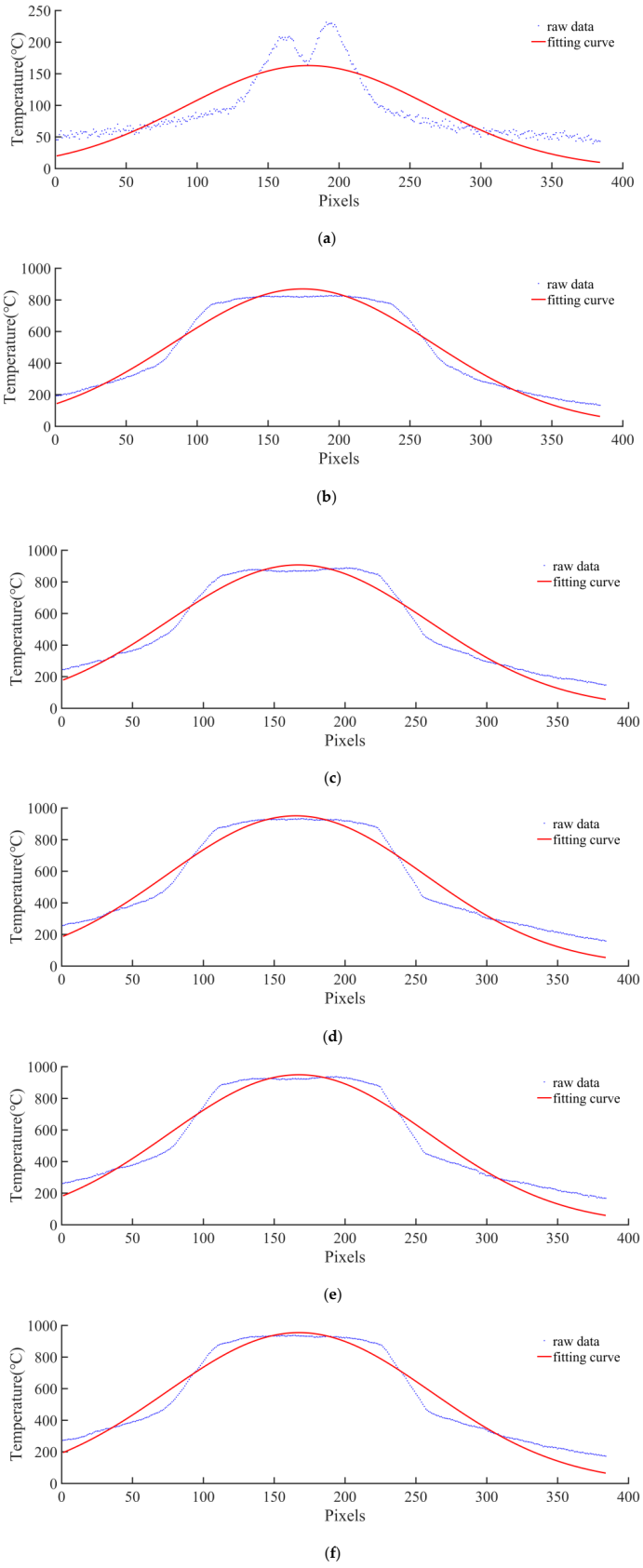

Figure 6. Gaussian fitting results of the temperature distribution of the weldment surface perpendicular to the welding direction at different times: (**a**) t = 4 s; (**b**) t = 8 s; (**c**) t = 12 s; (**d**) t = 20 s; (**e**) t = 25 s; (**f**) t = 29 s.

The mean absolute error of fitting the original temperature distribution data of the weldment surface perpendicular to the welding direction by quadratic fitting, cubic fitting, and Gaussian fitting is shown in Table 2.

Table 2. Fitting error of three fitting methods (°C).

Fitting Method \ Time	a	b	c	d	e	f
Quadratic fitting	29.6168	88.1995	103.7892	114.7833	114.1282	109.9440
Cubic fitting	28.5887	76.7988	81.8240	87.0293	91.3778	87.6424
Gaussian fitting	24.1636	41.1273	47.8991	51.8606	53.9904	51.0633

It can be found from Table 2 that the error of fitting the original temperature distribution data on the surface of the weldment perpendicular to the welding direction using the Gaussian fitting method was the smallest, and this conclusion was also verified in more infrared thermal images. According to the above conclusions, in the direction perpendicular to the welding direction, this paper proposed a feature extraction algorithm of the linear temperature distribution of the weldment surface based on Gaussian fitting. The extracted Gaussian fitting curve coefficient was adopted to represent the linear temperature distribution feature on the surface of the weldment perpendicular to the welding direction.

Secondly, the linear temperature distribution features of the weldment surface parallel to the welding direction were extracted. The temperature distribution on any straight line parallel to the welding direction can be considered as the temperature change experienced by any point on the straight line, that is, the thermal cycle process of that point. According to the above principles, this paper proposed an algorithm for extracting the linear temperature distribution features of the weldment surface based on the thermal cycle parameters, and the extracted welding thermal cycle parameters were used to represent the linear temperature distribution features of the weldment surface parallel to the welding direction. Figure 7 is the linear temperature distribution curve of the weldment surface parallel to the welding direction at different times. In this paper, two welding thermal cycle parameters, the maximum temperature and the cooling rate, were extracted from the measured welding thermal cycle curve to represent the linear temperature distribution features of the weldment surface parallel to the welding direction.

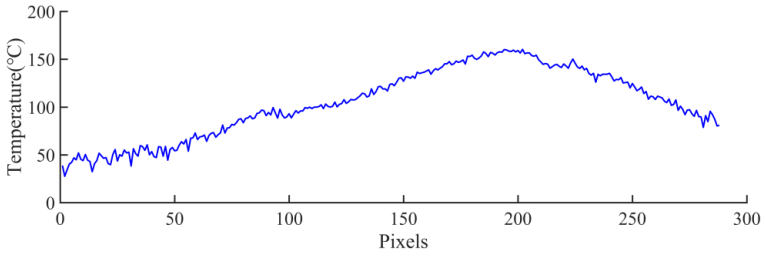

(**a**)

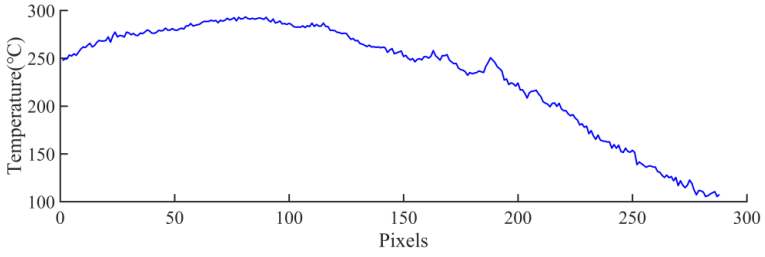

(**b**)

Figure 7. *Cont.*

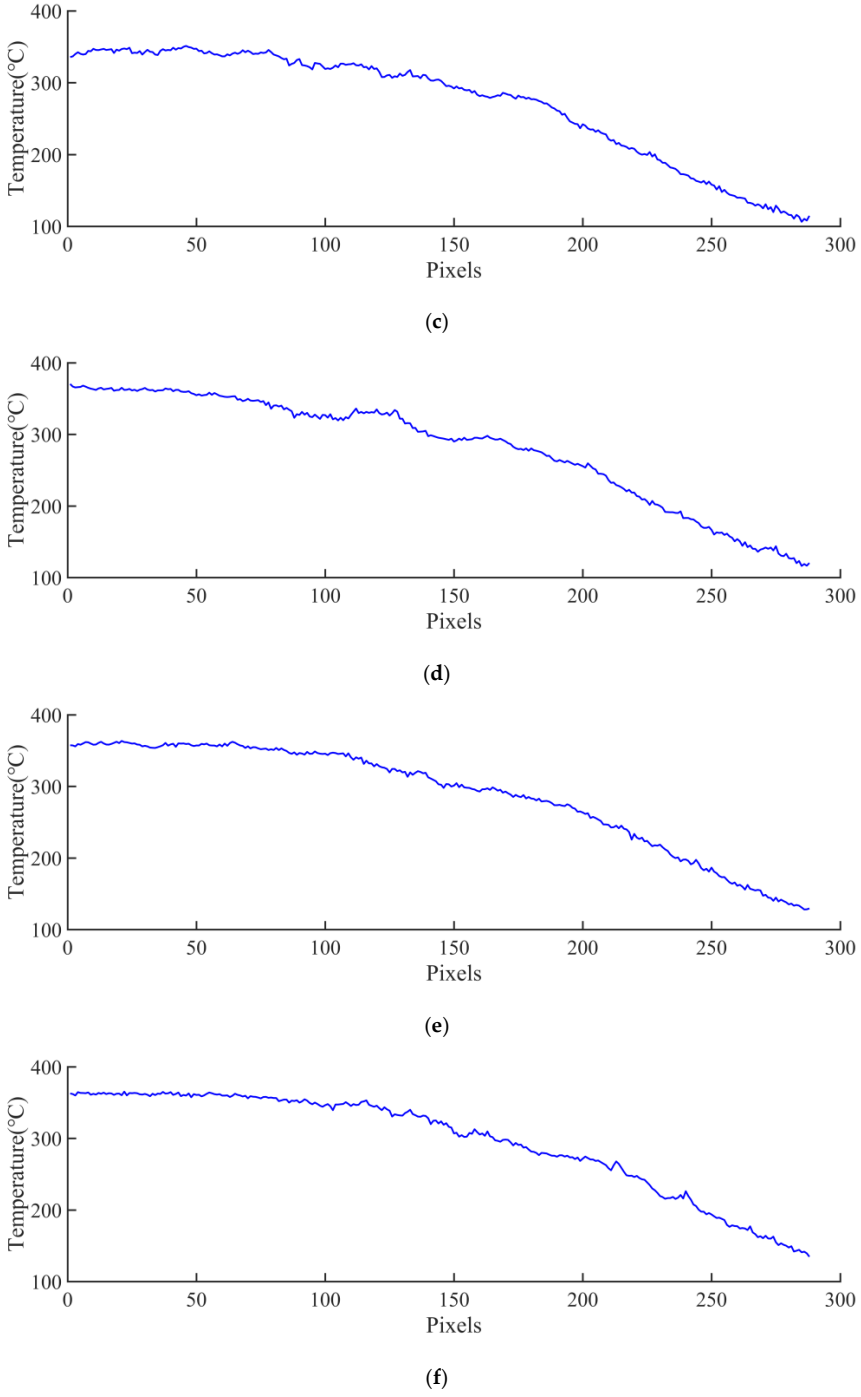

Figure 7. Linear temperature distribution curve of the weldment surface parallel to the welding direction at different times: (**a**) t = 4 s; (**b**) t = 8 s; (**c**) t = 12 s; (**d**) t = 20 s; (**e**) t = 25 s; (**f**) t = 29 s.

4. Feasibility Analysis of Identifying the Welding Penetration Using Linear Temperature Distribution Features

In this paper, a welding penetration sensing method for variable groove weldments based on an infrared sensor and an artificial neural network was put forward. The weld penetration was recognized by the linear temperature distribution features on the surface of the weldment, and a flow chart of this method is described in Figure 8.

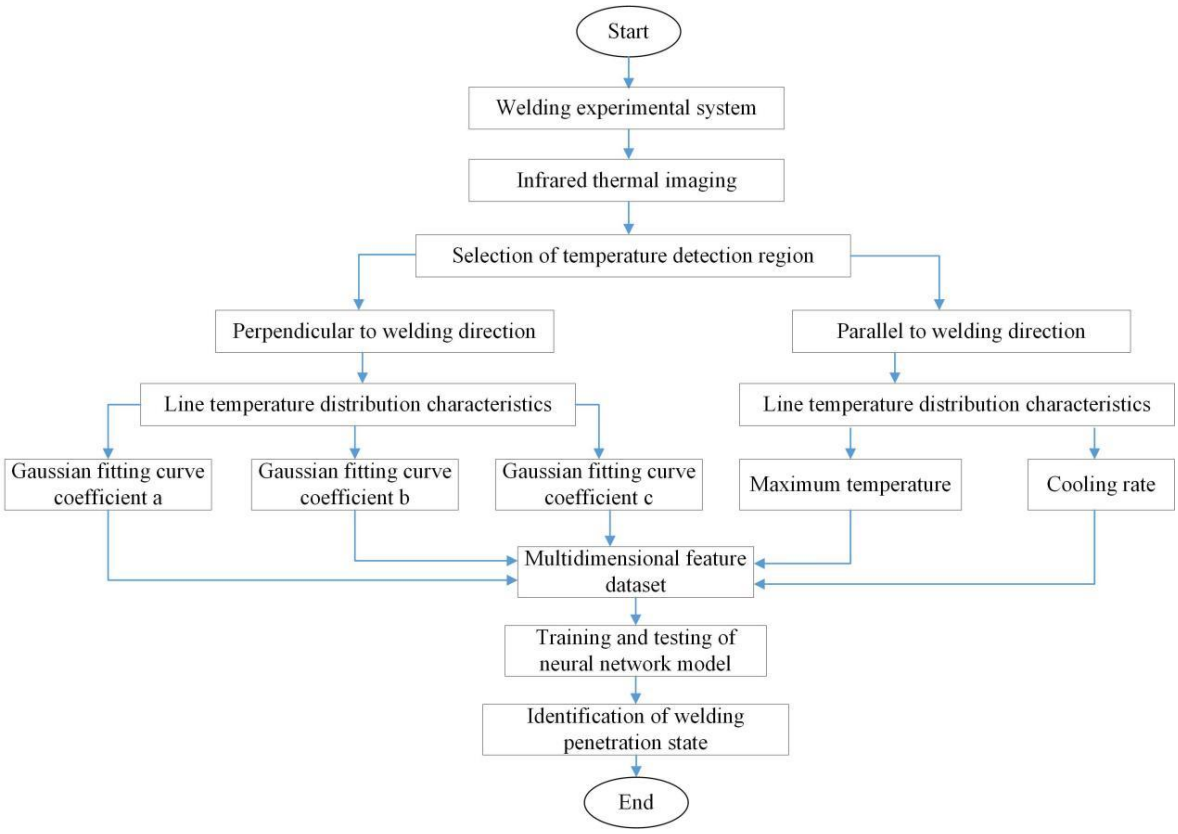

Figure 8. Flow chart of the proposed penetration sensing method.

For the sake of verifying the feasibility of using the extracted five-dimensional linear temperature distribution features on the surface of the weldment to identify the penetration of a variable groove weld, the principal component analysis (PCA) algorithm was adopted for reducing the five-dimensional temperature distribution features to three-dimensional features so as to realize the visualization. A total of 500 sets of nonpenetration state data, 900 sets of full penetration state data, and 100 sets of excessive penetration state data were extracted from the welding experiment, and the display results after the dimension reduction are shown in Figure 9. It can be found that most of the feature points corresponding to different penetration states were gathered together and could be well distinguished; only a small number of feature points overlapped. In general, the linear temperature distribution feature of the weldment surface under different penetration modes had certain separability, and the penetration of the variable groove weld could be diagnosed using the linear temperature distribution features of the weldment surface extracted in this paper.

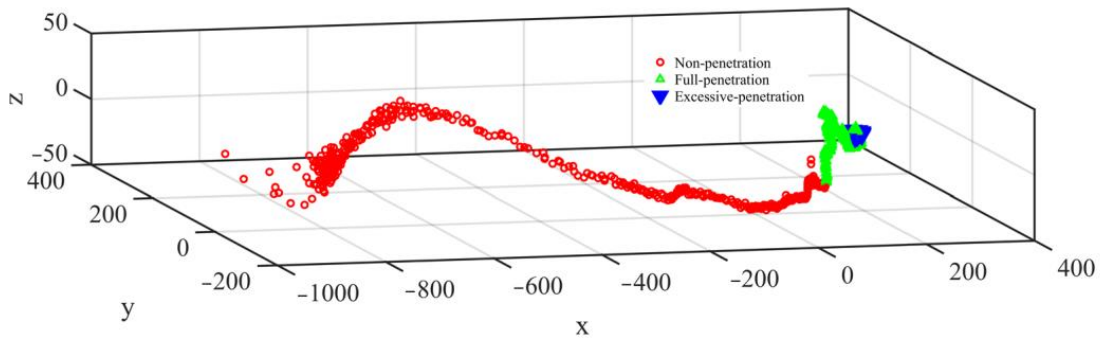

Figure 9. Display results of the linear temperature distribution features of the weldment surface after dimension reduction.

5. Welding Penetration Detection of a Variable Groove Weldment Based on an Artificial Neural Network

In this paper, by means of a BP neural network, a penetration recognition model for variable groove welds was established with the extracted five-dimensional linear temperature distribution features of the weldment surface as the input and the penetration of the variable groove weld as the output. There were three kinds of penetration states for a variable groove weld at the output end of the network model, and we used 0 to represent the nonpenetration state, 1 to represent the full penetration state, and 2 to represent the excessive penetration state. The number of hidden layers and the number of neurons in each layer of the penetration recognition model were closely related to the prediction accuracy of the recognition model. In accordance with the experimental test results, and the hidden layers of the recognition model were set as two layers, and each layer was set with 10 neurons. A structural diagram of the penetration recognition model for variable groove welds is shown in Figure 10. The activation function of the neural network was a sigmoid function, the training function was Trainlm, the maximum number of training times was 200, the learning rate was 0.01, and the target error was 0.001. The loss function of the neural network was the mean squared error (MSE), and its calculation equation is:

$$E = \frac{1}{2}\sum_{k}(y_k - t_k)^2 \tag{2}$$

where y_k is the output parameter of the neural network, and t_k is the target parameter of the neural network.

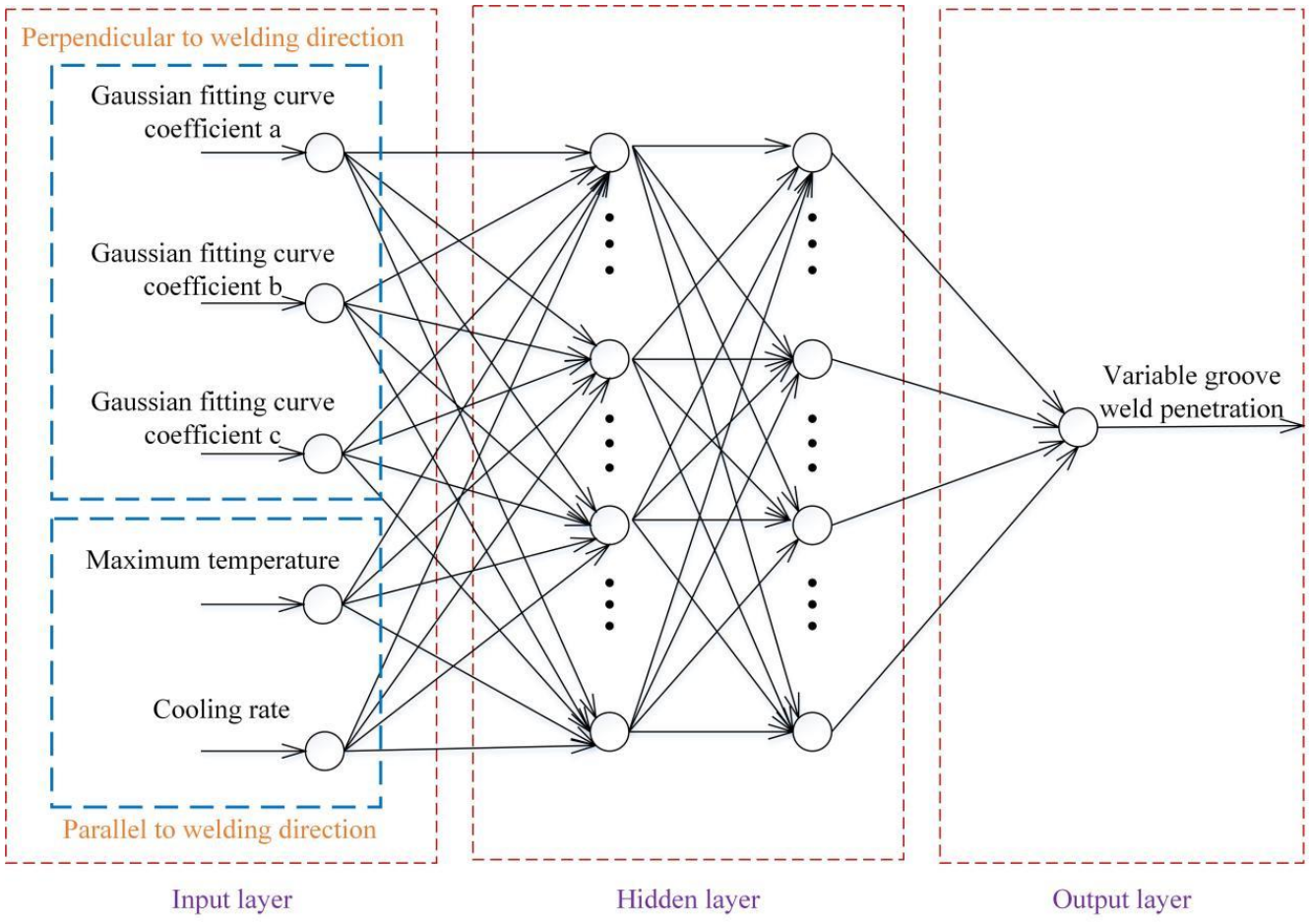

Figure 10. The structure of the penetration state recognition model for a variable groove weld.

Prior to training and testing the network model, the data set needed to be normalized. A total of 1500 sets of data were extracted from the experiment, 1200 sets of data were selected to form the training set, and the remaining 300 sets of data were used to form the test set. The recognition results of the penetration recognition model for a variable groove weld are shown in Figure 11, and the recognition accuracy is described in Table 3.

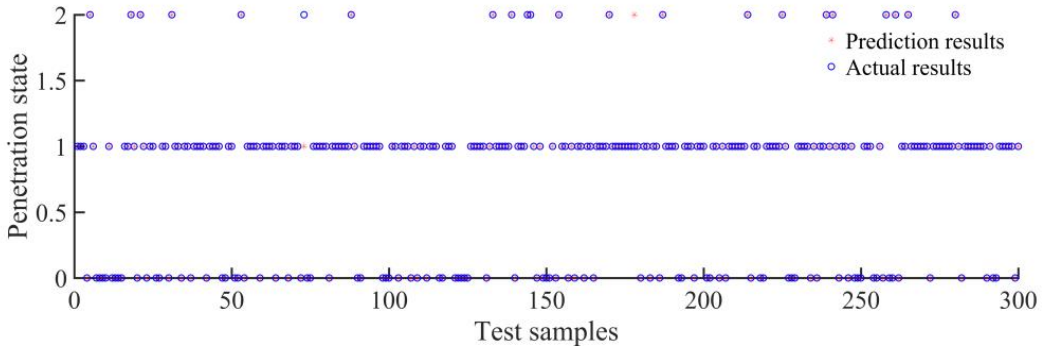

Figure 11. Recognition results of the penetration state.

Table 3. Recognition accuracy of the penetration state.

Penetration State	Nonpenetration	Full Penetration	Excessive Penetration
Recognition accuracy	100%	99.47%	95.45%

Gradually reducing the number of data sets in the training set, the number of data sets in the training set and the recognition accuracy of the penetration recognition model for variable groove welds are described in Table 4. It can be seen that the recognition accuracy of the penetration recognition model for the three penetration states remained above 92%.

Table 4. Recognition accuracy of the penetration state under different data sets of training set.

Training Set	Test Set	Nonpenetration	Full Penetration	Excessive Penetration
1000	500	99.42%	98.99%	96.88%
750	750	99.60%	98.45%	95.92%
500	1000	99.70%	97.84%	92.42%

When 50 sets of nonpenetration state data, 50 sets of full penetration state data, and 50 sets of excessive penetration state data were randomly selected to form a training set, and all 1500 sets of data extracted from the experiment were used to form a test set, the recognition results of the penetration recognition model for variable groove welds are shown in Figure 12, the recognition results of each penetration state are described in Table 5, and the recognition accuracy is described in Table 6.

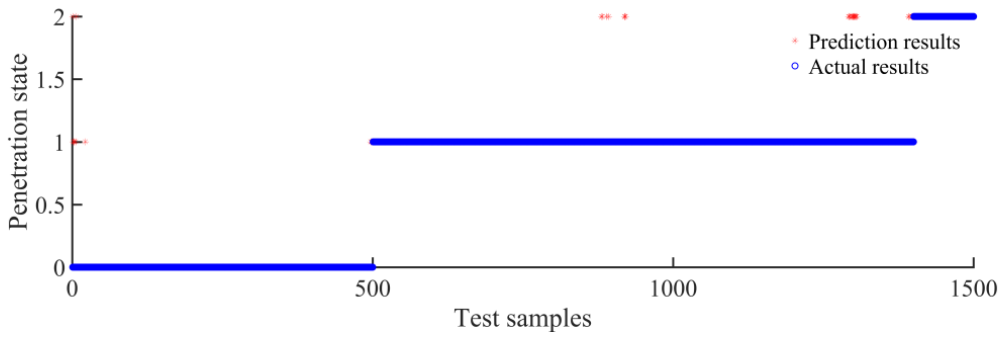

Figure 12. Recognition results of the penetration state by using another training method of recognition model.

Table 5. Prediction results of each penetration state by using BP neural network.

Prediction State \ Actual State	Nonpenetration	Full Penetration	Excessive Penetration
Nonpenetration	489	0	0
Full penetration	9	874	1
Excessive penetration	2	26	99

Table 6. Recognition accuracy of the penetration state by using BP neural network.

Penetration State	Nonpenetration	Full Penetration	Excessive Penetration
Recognition accuracy	97.80%	97.11%	99.00%

In addition, this paper also used the support vector machine (SVM) to establish a recognition model for variable groove weld penetration in accordance with the above training strategy. The recognition results of each penetration state are described in Table 7, and the recognition accuracy is described in Table 8.

Table 7. Prediction results of each penetration state by using SVM.

Prediction State \ Actual State	Nonpenetration	Full Penetration	Excessive Penetration
Nonpenetration	497	13	0
Full penetration	2	786	19
Excessive penetration	1	101	81

Table 8. Recognition accuracy of the penetration state by using SVM.

Penetration State	Nonpenetration	Full Penetration	Excessive Penetration
Recognition accuracy	99.40%	87.33%	81.00%

Through the above experimental results, it can be seen that the overall recognition accuracy of the recognition model for variable groove penetration based on a BP neural network was higher than that of the recognition model based on SVM. The recognition error of the recognition model for the variable groove weld penetration mainly occurred in the adjacent penetration state, which was due to the close welding temperature field in the adjacent penetration state at some moments. Moreover, the extraction and processing of the linear temperature distribution features also had some errors, which led to errors in the recognition of the weld penetration. In general, the method proposed in this paper can be extended to the online sensing of the penetration of variable groove weldments.

6. Conclusions

In this paper, a penetration sensing method for variable groove weldments based on an infrared sensor and an artificial neural network was proposed. The main conclusions are as follows:

1. A linear temperature distribution feature extraction algorithm based on Gaussian fitting was studied in the direction perpendicular to the welding direction, and a linear temperature distribution feature extraction algorithm based on the thermal cycle parameters was studied in the direction parallel to the welding direction, which could extract the temperature field distribution of the weldment surface to a certain extent.
2. The linear temperature distribution features in the welding heat-affected zone around the weld pool under different penetration states had a certain separability.
3. With the extracted linear temperature distribution features in the welding heat-affected zone around the weld pool as the input, a penetration recognition model for the variable groove weld was established based on an artificial neural network, which could realize the high-precision sensing of the three penetration states, such as nonpenetration, full penetration, and excessive penetration.

4. The welding penetration sensing method proposed in this paper solves the problem that the sensing of the welding penetration is affected by arc light to a large extent, and it provides a new method for the sensing of welding penetration.

Author Contributions: Conceptualization, R.Y.; methodology, R.Y.; writing-original draft preparation, R.Y.; investigation, Y.H. and S.Q.; validation, S.Q. and Y.P.; writing-review and editing, Y.H. and Y.P.; supervision, K.W.; project administration, K.W.; funding acquisition, R.Y., Y.H. and K.W. All authors have read and agreed to the published version of the manuscript.

Funding: This work was supported by the Guangdong Provincial Key Field Research and Development Program (2018B090906004), China Postdoctoral Science Foundation (2022M711627) and Natural Science Foundation of Jiangsu Province (BK20200497).

Institutional Review Board Statement: Not applicable.

Informed Consent Statement: Not applicable.

Data Availability Statement: Not applicable.

Conflicts of Interest: The authors declare no conflict of interest.

References

1. Sudhagar, S.; Sakthivel, M.; Ganeshkumar, P. Monitoring of friction stir welding based on vision system coupled with Machine learning algorithm. *Measurement* **2019**, *144*, 135–143. [CrossRef]
2. Zhao, D.; Wang, Y.; Liang, D.; Ivanov, M. Performances of regression model and artificial neural network in monitoring welding quality based on power signal. *J. Mater. Res. Technol.* **2019**, *9*, 1231–1240. [CrossRef]
3. Shen, B.; Lu, J.; Wang, Y.; Chen, D.; Han, J.; Zhang, Y.; Zhao, Z. Multimodal-based weld reinforcement monitoring system for wire arc additive manufacturing. *J. Mater. Res. Technol.* **2022**, *20*, 561–571. [CrossRef]
4. Zhang, X.; Yin, Z.; Xiong, Y. Edge Detection of the Low Contrast Welded Joint Image Corrupted by Noise. In Proceedings of the 2007 8th International Conference on Electronic Measurement and Instruments, Xi'an, China, 16–18 August 2007.
5. Deng, S.; Jiang, L.; Jiao, X.; Xue, L.; Cao, Y. Weld Seam Edge Extraction Algorithm Based on Beamlet Transform. In Proceedings of the 2008 Congress on Image and Signal Processing, Sanya, China, 27–30 May 2008. [CrossRef]
6. Shen, Z.; Sun, J. Welding seam defect detection for canisters based on computer vision. In Proceedings of the 2013 6th International Congress on Image and Signal Processing (CISP), Hangzhou, China, 16–18 December 2013.
7. Khumaidi, A.; Yuniarno, E.M.; Purnomo, M.H. Welding defect classification based on convolution neural network (CNN) and Gaussian kernel. In Proceedings of the 2017 International Seminar on Intelligent Technology and Its Applications (ISITIA), Surabaya, Indonesia, 28–29 August 2017.
8. Haffner, O.; Kučera, E.; Drahoš, P.; Cigánek, J. Using Entropy for Welds Segmentation and Evaluation. *Entropy* **2019**, *21*, 1168. [CrossRef]
9. Yu, R.; Bai, L. CMT penetration status prediction based on temperature field distribution of weld pool. *Optik* **2020**, *206*, 164301. [CrossRef]
10. Yusof, M.; Ishak, M.; Ghazali, M. Classification of weld penetration condition through synchrosqueezed-wavelet analysis of sound signal acquired from pulse mode laser welding process. *J. Mater. Process. Technol.* **2019**, *279*, 116559. [CrossRef]
11. Chen, C.; Lv, N.; Chen, S. Welding penetration monitoring for pulsed GTAW using visual sensor based on AAM and random forests. *J. Manuf. Process.* **2020**, *63*, 152–162. [CrossRef]
12. Sibillano, T.; Rizzi, D.; Mezzapesa, F.P.; Lugarà, P.M.; Konuk, A.R.; Aarts, R.; Veld, B.H.I.; Ancona, A. Closed Loop Control of Penetration Depth during CO_2 Laser Lap Welding Processes. *Sensors* **2012**, *12*, 11077–11090. [CrossRef]
13. Yang, J.; Wang, K.; Wu, T.; Zhou, X. Welding penetration recognition in aluminum alloy tandem arc welding based on visual characters of weld pool. *Trans. China Weld. Inst.* **2017**, *38*, 19–52.
14. Xia, Y.-J.; Zhou, L.; Shen, Y.; Wegner, D.M.; Haselhuhn, A.S.; Li, Y.-B.; Carlson, B.E. Online measurement of weld penetration in robotic resistance spot welding using electrode displacement signals. *Measurement* **2020**, *168*, 108397. [CrossRef]
15. Ren, W.; Wen, G.; Xu, B.; Zhang, Z. A Novel Convolutional Neural Network Based on Time–Frequency Spectrogram of Arc Sound and Its Application on GTAW Penetration Classification. *IEEE Trans. Ind. Informatics* **2020**, *17*, 809–819. [CrossRef]
16. Yu, R.; Kershaw, J.; Wang, P.; Zhang, Y. How to Accurately Monitor the Weld Penetration From Dynamic Weld Pool Serial Images Using CNN-LSTM Deep Learning Model? *IEEE Robot. Autom. Lett.* **2022**, *7*, 6519–6525. [CrossRef]
17. Liu, S.; Wu, D.; Luo, Z.; Zhang, P.; Ye, X.; Yu, Z. Measurement of pulsed laser welding penetration based on keyhole dynamics and deep learning approach. *Measurement* **2022**, *199*, 111579. [CrossRef]
18. Wikle, H.C.; Kottilingam, S.; Zee, R.H.; Chin, B.A. Infrared sensing techniques for penetration depth control of the submerged arc welding process. *J. Mater. Process. Technol.* **2001**, *113*, 228–233. [CrossRef]
19. Tan, X.; Zhang, H. Study on Numerical simulation of temperature field in welding process based on infrared measuring temperature technique. *Infrared Technol.* **2004**, *26*, 93–96.

20. Alfaro, S.; Franco, F.D. Exploring Infrared Sensoring for Real Time Welding Defects Monitoring in GTAW. *Sensors* **2010**, *10*, 5962–5974. [CrossRef]
21. Kafieh, R.; Lotfi, T.; Amirfattahi, R. Automatic detection of defects on polyethylene pipe welding using thermal infrared imaging. *Infrared Phys. Technol.* **2011**, *54*, 317–325. [CrossRef]
22. Zhu, J.; Wang, J.; Su, N.; Xu, G.; Yang, M. An infrared visual sensing detection approach for swing arc narrow gap weld deviation. *J. Mater. Process. Technol.* **2017**, *243*, 258–268. [CrossRef]
23. Guo, X. Ultrasonic Infrared Thermography of Aluminium Thin Plates for Crack Inspection in Friction Stir Welded Joints. *IEEE Sensors J.* **2020**, *20*, 6524–6531. [CrossRef]
24. Górka, J.; Jamrozik, W. Enhancement of Imperfection Detection Capabilities in TIG Welding of the Infrared Monitoring System. *Metals* **2021**, *11*, 1624. [CrossRef]
25. Pal, S.; Pal, S.K.; Samantaray, A.K. Artificial neural network modeling of weld joint strength prediction of a pulsed metal inert gas welding process using arc signals. *J. Mater. Process. Technol.* **2008**, *202*, 464–474. [CrossRef]
26. Wan, X.; Wang, Y.; Zhao, D.; Huang, Y.; Yin, Z. Weld quality monitoring research in small scale resistance spot welding by dynamic resistance and neural network. *Measurement* **2017**, *99*, 120–127. [CrossRef]
27. Zhang, Z.; Wen, G.; Chen, S. Weld image deep learning-based on-line defects detection using convolutional neural networks for Al alloy in robotic arc welding. *J. Manuf. Process.* **2019**, *45*, 208–216. [CrossRef]
28. Moslemi, N.; Gohari, S.; Abdi, B.; Sudin, I.; Ghandvar, H.; Redzuan, N.; Hassan, S.; Ayob, A.; Rhee, S. A novel systematic numerical approach on determination of heat source parameters in welding process. *J. Mater. Res. Technol.* **2022**, *18*, 4427–4444. [CrossRef]
29. Luo, H.; Zeng, H.; Hu, L.; Hu, X.; Zhou, Z. Application of artificial neural network in laser welding defect diagnosis. *J. Mater. Process. Technol.* **2005**, *170*, 403–411. [CrossRef]
30. Hong, Y.; Liu, S.; Xu, C.; Liu, F.; Zhang, H. The Calculation of Laser-Arc Hybrid Weld Bead Shape Basing on Multiple Population Genetic Algorithm and Neural-networks. *Appl. Laser* **2015**, *35*, 677–683.
31. Lei, Z.; Shen, J.; Wang, Q.; Chen, Y. Real-Time weld geometry prediction based on multi-information using neural network optimized by PCA and GA during thin-plate laser welding. *J. Manuf. Process.* **2019**, *43*, 207–217. [CrossRef]
32. Li, H.; Liu, J.; Xie, J.; Wang, X. GTAW Penetration Prediction Model Based on Convolution Neural Network Algorithm. *J. Mech. Eng.* **2019**, *55*, 22–28.
33. Bacioiu, D.; Melton, G.; Papaelias, M.; Shaw, R. Automated defect classification of Aluminium 5083 TIG welding using HDR camera and neural networks. *J. Manuf. Process.* **2019**, *45*, 603–613. [CrossRef]
34. Hartl, R.; Bachmann, A.; Habedank, J.; Semm, T.; Zaeh, M. Process Monitoring in Friction Stir Welding Using Convolutional Neural Networks. *Metals* **2021**, *11*, 535. [CrossRef]
35. Yu, R.; Han, J.; Bai, L.; Zhao, Z. Identification of butt welded joint penetration based on infrared thermal imaging. *J. Mater. Res. Technol.* **2021**, *12*, 1486–1495. [CrossRef]